Optics Communications 501 (2021) 127343

Contents lists available at ScienceDirect

Optics Communications

journal homepage: www.elsevier.com/locate/optcom

Numerical analysis of low-RI WGM resonators excited by a periodically arranged multilayer dielectric planar waveguide

Meng Zhang [a], Jiansheng Liu [a,*], Jiangtao Cheng [b]

[a] School of Electronic and Information Engineering, Beihang University, 37 Xueyuan Road, Beijing 100191, China
[b] Department of Mechanical Engineering, 635 Prices Fork Road, Virginia Tech, VA 24061, USA

ARTICLE INFO

Keywords:
Integrated optics device
BSW planar waveguide
Whispering gallery mode resonance
Optical coupling

ABSTRACT

In the applications of whispering gallery mode (WGM) resonators, especially those with low refractive indices (RIs), optical excitation is always a critical issue due to the lack of suitable and matching waveguide materials. The Bloch surface wave (BSW) can facilitate achieving an effective coupling, resulting from its field distribution extending a large portion of its mode energy around the external surface and its easy adjustment of the effective refractive index. In this paper, a BSW waveguide platform for adaptive excitation of spherical WGM resonators is proposed, designed, and numerically analyzed. The simulation results show that the WGM resonator stimulated by BSW exhibits a resonance depth (RD) as large as ~98% and a high total quality factor Q_{total} ~3.13×10^4 which is in the same order of magnitude as its intrinsic value $Q_{intrinsic}$ of 5.8×10^4. Moreover, less limited by its constitutive materials, this BSW-WGM platform is robust and especially suitable for fully integrated applications.

1. Introduction

During the past two decades, many WGM-based applications that call for ultra-narrow line-widths, large energy densities, or fine sensing of environmental changes have been put forward and demonstrated [1,2]. In terms of sensing, the low RI (such as SiO_2 [3], MgF_2 [4], PDMS [5], etc.) WGM resonators placed in an aqueous environment can induce a low RI contrast between the resonator and the surrounding medium (water), which results in the evanescent field of the resonator penetrating deep into the analyte solution. Therefore, the WGM resonators with low RIs can further enhance the analyte-cavity interactions and have great potential in high-sensitivity sensors. On the other hand, in the applications of WGM resonators, especially those with low RIs, an efficient excitation mechanism is of crucial importance. Numerous optical devices including standard tapered fiber [6,7], thick tapered fiber [8,9], optical fiber half-coupler [10,11], prism coupler (triangular or hemispherical) [12–14], conventional cladding-core-cladding planar waveguide [15], and photonic chip optical waveguide [16,17] have been utilized to couple light into WGM resonators. Among these couplers, the standard tapered fiber coupling is one of the most popular techniques and shows a very high coupling efficiency (~100%), but its fragility prevents this coupling protocol from practical applications. Even though all the thick tapered fiber, the optical fiber half-coupler and the prism coupling methodologies are relatively robust techniques, both the standard fiber and the thick tapered fiber coupling methods necessitate high alignment accuracy, not to mention the fact that the optical fiber half-coupler falls short of phase-match control and the prism coupler fails to make the guided-wave control. Moreover, although the conventional planar waveguides consisting of cladding, waveguide layer, and substrate are robust and widely used in integrated photonic applications, they are excluded from exciting the resonators with lower RIs due to the lack of suitable waveguide constitutive materials. Recently, the photonic chip optical waveguide has been proved to be an efficient coupling technique to the low-RI MgF_2 resonators [16], but it entails a motor-driven stage of nano precision to control the air gap thickness between the resonator and the waveguide for a good coupling. In this paper, we propose, design, and numerically analyze a novel planar waveguide that consists of a periodically arranged dielectric multilayer for the fully integrated and effective excitation of low RI WGM resonators.

2. Working principle

The proposed periodically arranged multilayer dielectric planar waveguide, which is the so called BSW waveguide, supports a special propagating mode known as the BSW whose propagation is confined adjacent to the surface of the multilayer waveguide [18–28]. This confined mode is similar to the surface plasmon wave at the metal/dielectric interface [29]. Unlike the surface plasmon wave suffering from high metal absorption loss, the BSW greatly reduces loss due to

* Corresponding author.
E-mail address: jsliu@buaa.edu.cn (J. Liu).

https://doi.org/10.1016/j.optcom.2021.127343
Received 2 May 2021; Received in revised form 25 July 2021; Accepted 3 August 2021
Available online 5 August 2021

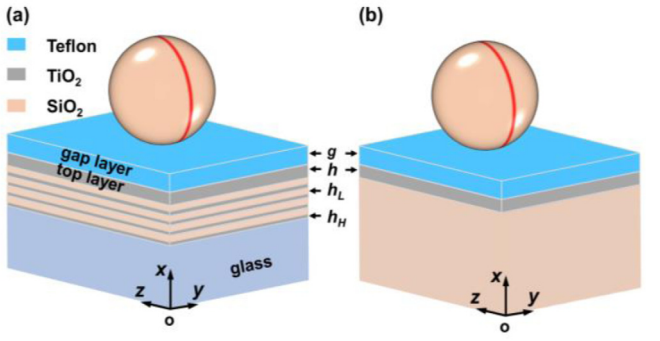

Fig. 1. (a) The 3D sketch of the WGM excitation scheme based on the BSW multilayer waveguide. (b) The 3D sketch of the WGM excitation scheme based on the conventional planar waveguide. The red line indicates the trajectory of the WGMs.

the all-dielectric environment. The BSW can confine a significant portion of its mode energy in the surrounding external medium, which can significantly enhance the light-mater interaction strength and therefore lead to a wide range of applications. For instance, the BSW has been intensively studied as highly sensitive biochemical sensors in recent years [20,25,26,30]. This feature of strong mode energy confinement also offers an effective pathway for BSW to exchange energy with nearby optical devices due to the sufficient mode overlapping between the BSW and the mode in external devices. Importantly, assisted by tuning the thicknesses of the dielectric layers, this unique property of BSW enables its effective RI to approach and match the RI of the to-be-coupled optical devices with relatively low RI. This excitation protocol is quite different from the conventional cladding-core-substrate planar waveguide, in which the effective RI of its mode cannot be smaller than that of the substrate.

Fig. 1a shows the schematic of the excitation of a low RI spherical WGM microcavity resonator on the BSW waveguide. The BSW waveguide consists of a top dielectric layer placed on the one-dimensional (1D) periodical multilayered structure. The 1D dielectric stack has a finite number of periods composed of alternating layers of materials with low and high RIs, respectively, which are sequentially deposited on a glass slide. With a proper design, the proposed multilayer planar waveguide could generate the desired BSW for exciting the WGMs in the low RI microcavity on the waveguide. The microcavity can be a microsphere cavity, a cylinder cavity, or other shaped cavities. In this paper, the spherical microcavity is sampled to evaluate the BSW-WGM excitation protocol by the proposed BSW waveguide consisting of multilayered structures. A solid gap layer is sandwiched between the top layer and the microcavity for adjusting the mode overlap between the BSW waveguide and the WGM resonator and achieving fully integration of the waveguide and the resonator. Additionally, in order to demonstrate the advantages of exciting WGMs by BSW waveguide, the WGM excitation based on a conventional planar waveguide, in which the 1D periodical multilayers are replaced by a single layer as shown in Fig. 1b, is also analyzed for comparison purpose.

3. Device design

3.1. Properties of the WGMs in the microsphere resonators

In this work, as the multilayered BSW waveguide is used to stimulate the WGMs in a spherical cavity, the coupling requirements and conditions between them should be first elaborated. In this respect, the main factors that determine the coupling efficiency are the effective-refractive-index matching and the field overlapping between the WGMs of the resonator and the BSW of the BSW waveguide. Therefore, both the effective refractive index n_{eff} and the field distribution of the WGMs of the spherical cavity need to be matched. Meanwhile, the

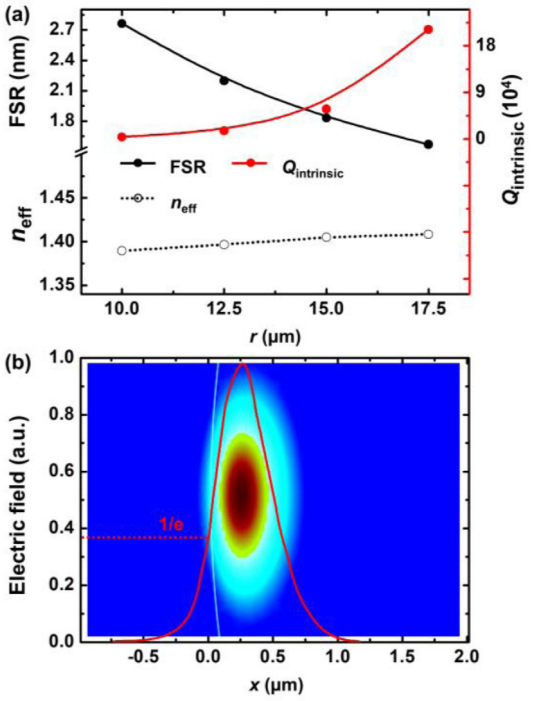

Fig. 2. (a) Evolutions of the effective refractive index n_{eff}, the intrinsic quality factor $Q_{\mathrm{intrinsic}}$ and FSR of the mode closest to 500 nm wavelength with the microsphere radius r. (b) The fundamental WGM mode profile.

quality factor Q and the free spectra range (FSR), which are important merit factors of a resonant cavity, also need to be evaluated. Here, silicon dioxide (SiO_2), a dielectric material with a low refractive index $n_{SiO_2} = 1.4553$, is selected as the material of the microsphere cavity. Considering that biological samples (such as Influenza A virus particles) are generally contained in aqueous solutions, water with $n_c = 1.33–5.16 \times 10^{-5}$i is taken as the medium surrounding the microsphere cavity, which is also conductive to the real applications of high-sensitivity sensing. The light wavelength is chosen at ~500 nm locating at the weak absorption band of the aqueous solutions. Given that the fundamental WGM has the highest intrinsic quality factor, only the fundamental WGM is considered in this work. Using the finite element method (FEM), n_{eff}, $Q_{\mathrm{intrinsic}}$, FSR and the field distribution of the fundamental WGM in the SiO_2 microcavity can be obtained. The variations of n_{eff}, $Q_{\mathrm{intrinsic}}$, and FSR with the microsphere radius r in the range of 10 μm to 17.5 μm are shown in Fig. 2a and the fundamental WGM mode profile is shown in Fig. 2b. It can be seen that n_{eff} of the WGM is around 1.4 and $Q_{\mathrm{intrinsic}}$ increases exponentially from 3.78×10^3 to 2.31×10^5 with r increasing from 10 μm to 17.5 μm, indicating that a larger microsphere cavity would have a higher $Q_{\mathrm{intrinsic}}$. This observation provides a criterion to evaluate the WGM excitation protocol by simply comparing $Q_{\mathrm{intrinsic}}$ with the total quality factor Q_{total}.

3.2. Design of the BSW planar waveguide for WGM coupling

Next, the BSW planar waveguide for coupling with WGMs is designed and optimized on the principle of effective RI matching and mode field distribution overlapping. From the design perspective of the BSW waveguide, the materials and the geometry of its periodic structure and the top layer above the waveguide are the most important factors affecting the properties of the BSW waveguide [24]. Therefore, the subsequent waveguide design and performance optimization are based on these aspects.

The commercially available titanium dioxide (TiO_2, $n_H = 2.5512$) and silicon dioxide (SiO_2, $n_L = 1.4553$) are selected as the high RI

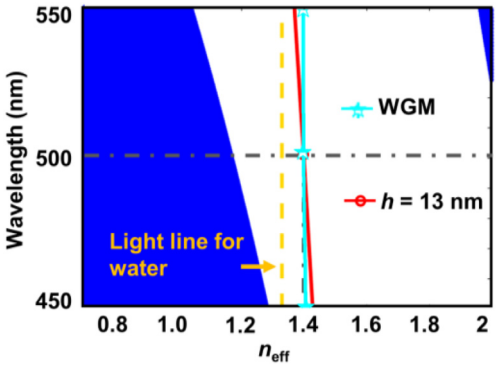

Fig. 3. PBG for the BSW waveguide. The white zone is the forbidden band. The dispersion relations for the BSW with the top layer thickness h = 13 nm and for the WGM with r = 15 μm are also shown. The dashed yellow line denotes the light line in water. The cross-point of the two gray lines indicates the desired n_{eff} for matching RI between the BSW and the WGMs.

and low RI materials of the periodic waveguide structure, respectively. As mentioned in Section 3.1, aqueous solutions are assumed as the surrounding medium. In order to locate the region where the BSW can exist, firstly, the photonic band-gap (PBG) or the forbidden band of the periodic structure need to be determined by the parameters of the periodic structure. Using the theory provided in [31], the structure parameters of a 4-period stack with h_H = 87 nm (TiO_2) and h_L = 135 nm (SiO_2) as the thicknesses of the high RI and low RI layers, respectively, are obtained. Then the PBG of the period structure is calculated by the transfer matrix method and is shown as the white region in Fig. 3. Besides, as the BSW waveguide is covered by aqueous solutions, the BSW dispersion curves should reside at the right side of the water light line (dashed yellow line in Fig. 3) and in the PBG region. Moreover, since the effective refractive index n_{eff} of the WGMs is ~1.4, the BSW dispersion curves should be also around 1.4 for matching that of the WGMs. To make the waveguide support BSW with $n_{eff} \approx 1.4$, we need to properly design the thickness h of the top layer. Based on FEM calculation and according to the desired value of $n_{eff} \approx 1.4$, the thickness h of the top layer is determined to be ~13 nm as shown in Fig. 3.

The effect of the top layer thickness h on the n_{eff} of the BSW should be studied for evaluating its influence on the WGMs excitation by the BSW waveguide and on the fabrication tolerance of the top layer. The variations of n_{eff} of the 1D multilayer BSW waveguide with its top layer thickness h (red line) are plotted in Fig. 4a. The n_{eff} of the conventional waveguide is also shown in Fig. 4a (black dotted line). Since the substrate of the conventional waveguide is made of silica with a low RI, the effective RI of the TE_0 mode in the conventional waveguide is larger than that of the silica (dash-dotted yellow line in Fig. 4a). Thus, the conventional waveguide provides an effective index range to match the WGMs with n_{eff} larger than the index of silica. That is, it cannot efficiently excite the microcavity with n_{eff} smaller than the RI of silica. The n_{eff} of the BSW can be designed smaller or larger than the RI of silica, which is less limited by its constitutive materials. Obviously, BSW provides a wider range of effective index for matching that of the silica microcavity. Moreover, by scrutinizing the mode field profiles of the BSW and the TE_0 mode, two conclusions can be obtained. First, the top layer thickness h of the BSW waveguide has a substantial impact on the penetration depth of the BSW while the thickness h of the conventional waveguide has less influence on the penetration depth of the TE_0 mode. Second, at the same h, the BSW squeezes more mode energy outwards and penetrates deeper into the external medium (see Fig. 4b, c and d), which facilitates its mode overlapping with that of the WGMs. In summary, the above analyses show that the BSW waveguide can not only provide a wider effective index range for matching the n_{eff} of WGMs, but also enable more sufficient mode overlap between

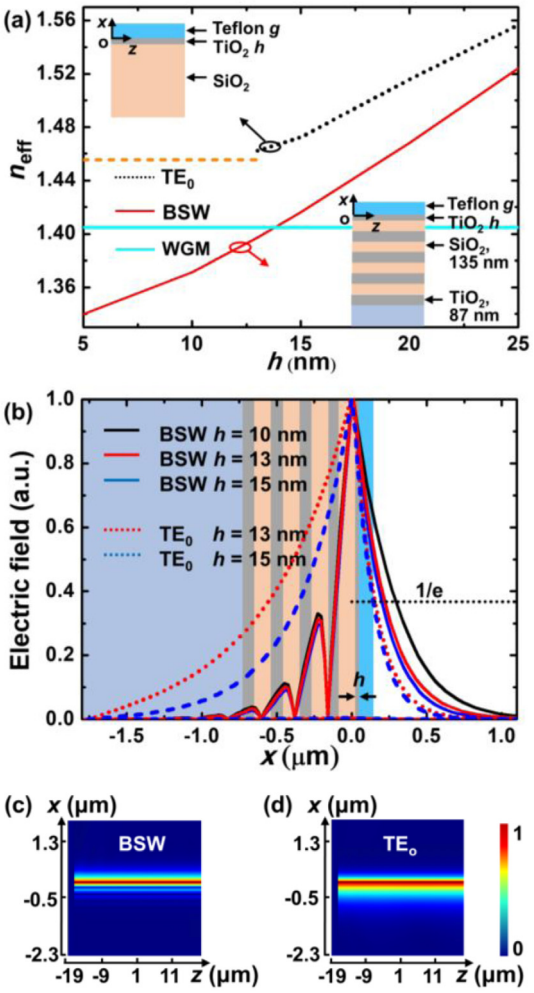

Fig. 4. (a) Effective RI for the BSW (red line), and that for the TE_0 mode (dotted black line) with respect to the top layer thickness h. The dashed yellow line is the boundary of the effective RI for the TE_0 mode. The light blue line is the effective refractive index n_{eff} of the WGMs with r = 15 μm. (b) The BSW mode profiles along x direction at h = 10 nm (black line), h = 13 nm (red line), and h = 15 nm (blue line), respectively and the TE_0 mode profiles along the x direction at h = 13 nm (dotted red line), and h = 15 nm (dotted blue line), respectively. (c) The BSW mode profiles at h = 13 nm. (d) The TE_0 mode profiles at h = 13 nm.

the BSW and the WGMs, indicating that the BSW is most suitable to stimulate the WGMs of spherical microcavities with a low RI.

4. WGMs excitation via BSW

In real applications, a properly designed BSW waveguide is highly desired for stimulating WGMs with high efficiency. Instead of $Q_{intrinsic}$, it is the total quality factor Q_{total}, which also takes optical coupling process into account, that is adopted by us in evaluating a practical micro resonator system. The degree of optical coupling, i.e., the percentage of input light involved in coupling, can be quantitatively reflected by the resonance depth RD [32]. To demonstrate and evaluate this excitation protocol, the optical properties including Q_{total} and RD of the WGM system based on the BSW waveguide are studied in this work. An efficient WGM system is featured with a sharp and deep resonance, i.e., a high Q_{total} and a deep RD. According to the coupling theory of micro resonator, the introduction of optical coupling makes Q_{total} less than $Q_{intrinsic}$, and in the under-coupling region, Q_{total} decreases with the increase of the coupling degree as reflected by RD [32]. From the perspective of energy coupling, a larger RD is expected. However, to

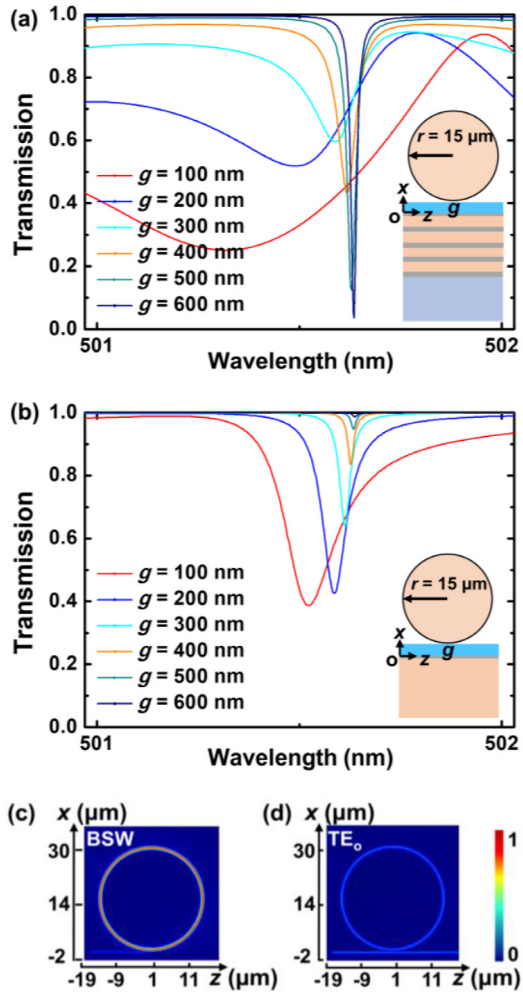

Fig. 5. The evolutions of the transmission spectra for (a) the BSW mode and (b) the TE_0 mode with the gap thickness g. The resonant mode field distributions for (c) the BSW with $g = 600$ nm and (d) the TE_0 with $g = 600$ nm.

maintain the high-quality factor characteristics of the micro resonator as much as possible after coupling, a larger Q_{total}, which is inversely proportional to RD, is more preferred. Therefore, in order to comprehensively evaluate the influences of these two factors on coupling efficiency, the figure of merit (FOM) is defined by us as the product of RD and Q_{total} so that a large FOM implies a high coupling efficiency. In general, except for some applications such as cavity QED [33], the system is always tuned close to or at the critical coupling (RD = 100%, $Q_{total} = 0.5\ Q_{intrinsic}$) to simultaneously achieve a high Q_{total} and a deep RD [16].

Besides, since the fundamental WGM of a microsphere is equivalent to that of a two-dimensional (2-D) microdisk [34], we used 2-D Finite-difference time-domain (FDTD) to study the coupling properties between the WGM and the BSW. The mode of the BSW waveguide is taken as the excitation source launching at the input port of the BSW waveguide. Then the BSW propagates along the BSW waveguide towards the microsphere cavity and eventually couples to it to excite the WGMs of the microsphere cavity.

Ideally, the thickness g of the gap layer between the WGM resonator and the BSW waveguide can modulate the strength of the mode overlap between the WGMs and the BSW. Thus, it is necessary to investigate the impact of the gap layer thickness g on Q_{total} and RD. In this study, Teflon with $n_g = 1.35$ is selected as the material of the gap layer. In Section 3, it has been predicted that the BSW waveguide with h~13 nm is suitable to stimulate the WGMs in the microsphere resonator with

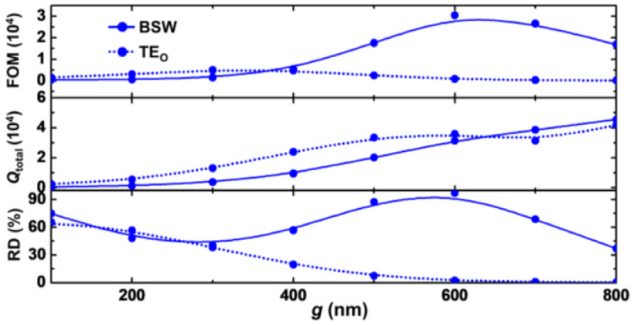

Fig. 6. The evolutions of the RD, Q_{total} and FOM for the BSW waveguide system (solid lines) and the conventional waveguide system (dotted lines) with the gap thickness g.

$r = 15$ μm. Fig. 5a shows the transmission spectra of the microsphere resonator with r~15 μm excited by the BSW waveguide with h~13 nm. As a comparison, the transmission spectra of the same microsphere resonator stimulated by a conventional waveguide with a thickness h~13 nm is depicted in Fig. 5b. It should be noted that h~13 nm is the cutoff thickness of the conventional waveguide. Here, the effective refractive index n_{eff} of the conventional waveguide reaches its minimum value, which is also the n_{eff} value closest to that of the WGM and is used in simulation (see Fig. 4a). From the transmission spectra, the resonant wavelength can be estimated and then the mode field distributions at this resonant wavelength can be obtained (Fig. 5c and d). Moreover, from the transmission spectra, the RD, the Q_{total} (defined by the ratio of the resonance wavelength to the full width at the half-maximum of a resonant peak), and the FOM can also be obtained (Fig. 6). The RD and the Q_{total} can be tuned by the gap thickness g, i.e., the degree of the mode overlap between the WGM and the BSW. With the gap thickness g~600 nm, the WGM excitation based on the BSW waveguide allows for a large RD approaching 98% while simultaneously provides a high Q_{total} of 3.13×10^4, which is near the critical coupling and in the same order of magnitude as the $Q_{intrinsic}$ of 5.8×10^4. In contrast, the WGMs stimulated by the conventional waveguide exhibit a much poorer performance. As such, the conventional waveguide system cannot simultaneously provide a high Q_{total} and a deep RD, leading to a poor mode field distribution at the resonant wavelength (see Fig. 5c and d). The FOM of the BSW waveguide system is about 5 times that of the conventional waveguide system. These traits can be mainly attributed to the following two aspects. First, the BSW waveguide allows its n_{eff} to go below the RI of silica, which can match the n_{eff} of the WGMs in the silica microcavity, whereas the n_{eff} of the conventional waveguide is always larger than the RI of silica. Second, the mode field profile of the BSW is conductive to enhancing the mode overlap. Moreover, our analyses show that the FOM of the BSW-WGM system does not obviously change with g in the range of 500 nm – 700 nm and maintains almost the largest value therein, allowing a large fabrication tolerance of the BSW waveguide.

5. Conclusions

In this work, we numerically studied the mechanisms of WGMs excitation by the BSW waveguide and unveiled BSW's excellent capability in stimulating WGMs in microcavities with relatively low refractive indices. The BSW waveguide can extend a large portion of its mode energy to its external surrounding medium, which is conductive to the sufficient overlap between the BSW and the WGMs and therefore the generation of low n_{eff} matching that of the WGMs. Compared with the conventional waveguide coupling protocol, the ultra-thin top layer on the 1D periodical multilayer waveguide is less limited by its constitutive materials and is apt to excite the low RI WGM resonators. Moreover, the BSW waveguide can simultaneously offer a deep RD as large as ~98% and a quality factor Q_{total} as high as $\sim 3.13 \times 10^4$, which is in the same order of magnitude as the $Q_{intrinsic}$, in stimulating the WGMs in low refractive index microresonators.

Declaration of competing interest

The authors declare that they have no known competing financial interests or personal relationships that could have appeared to influence the work reported in this paper.

Acknowledgments

This work is supported by National Natural Science Foundation of China (61775008) and National Science Foundation of USA (NSF ECCS 1808931).

References

[1] K.J. Vahala, Nature 424 (2003) 839–846.
[2] J. Yu, J. Zhang, R. Wang, A. Li, M. Zhang, S. Wang, P. Wang, J.M. Ward, S.N. Chormaic, Opt. Express 28 (2002) 32858–32868.
[3] F. Vollmer, S. Arnold, D. Keng, Proc. Natl. Acad. Sci. 105 (2009) 20701–20704.
[4] R. Zeltner, F. Sedlmeir, G. Leuchs, H.G.L. Schwefel, Eur. Phys. J. Spec. Top. 223 (2014) 1989–1994.
[5] C.H. Dong, L. He, Y.F. Xiao, V.R. Gaddam, S.K. Ozdemir, Appl. Phys. Lett. 94 (2009) 231119.
[6] M. Cai, O. Painter, K.J. Vahala, P.C. Sercal, Optim. Lett. 25 (2000) 1430–1432.
[7] Y. Yin, T. Nie, M. Ding, IEEE Sens. J. 20 (2020) 9871–9876.
[8] D. Farnesi, F. Chiavaioli, F. Baldini, G.C. Righini, S. Soria, C. Trono, G. Nunze Conti, Opt. Express 23 (2015) 21175–21180.
[9] D. Farnesi, F. Chiavaioli, F. Baldini, G.C. Righini, S. Soria, C. Trono, G. Nunze Conti, Optim. Lett. 39 (2014) 6525–6528.
[10] A. Serpengüzel, S. Arnold, G. Griffel, J.A. Lock, J. Opt. Soc. Amer. B 14 (1997) 790–795.
[11] N.M. Hanumegowda, I.M. White, X. Fan, Sensors Actuators B 120 (2006) 207–212.
[12] F. Sedlmeir, M.R. Foreman, U. Vogl, R. Zeltner, G. Schunk, D.V. Strekalov, C. Marquardt, G. Leuchs, H.G.L. Schwefel, Phys. Rev. Appl. 7 (2017).
[13] M. Zhang, W. Cheng, Z. Zheng, J. Cheng, J. Liu, Microfluid. Nanofluid. 23 (2019) 106.
[14] A.E. Shitikov, I.A. Bilenko, N.M. Kondratiev, V.E. Lobanov, A. Markosyan, M.L. Gorodetsky, Optica 5 (2018) 1525–1528.
[15] I.M. White, J.D. Suter, H. Oveys, X. Fan, T.L. Smith, J. Zhang, B.J. Koch, M.A. Haase, Opt. Express 15 (2007) 646–651.
[16] M. Anderson, N.G. Pavlov, J.D. Jost, G. Lihachev, J. Liu, T. Morais, M. Zervas, M.L. Gorodetsky, T.J. Kippenberg, Optim. Lett. 43 (2018) 2106–2109.
[17] L. An, Z. Zheng, Z. Li, T. Zhou, J.T. Cheng, Opt. Commun. 282 (2009) 3266–3269.
[18] L. Yu, E. Barakat, W. Nakagawa, H.P. Herzig, J. Opt. Soc. Amer. B 31 (2014) 2996–3000.
[19] R. Wang, H. Xia, D. Zhang, J. Chen, L. Zhu, Y. Wang, E. Yang, T. Zang, X. Wen, G. Zou, Nature Commun. 8 (2017) 14330.
[20] A. Angelini, A. Lamberti, S. Ricciardi, F. Frascella, P. Munzert, N. De Leo, E. Descrovi, Optim. Lett. 39 (2014) 6391–6394.
[21] A. Sinibaldi, N. Danz, E. Descrovi, P. Munzert, U. Schulz, F. Sonntag, L. Dominici, F. Michelotti, Sensors Actuators B 174 (2012) 292–298.
[22] E. Gonzalez-Valencia, R.A. Herrera, P. Torres, Opt. Express 27 (2019) 8236–8245.
[23] T. Tu, F. Pang, Z. Shan, J. Cheng, H. Liu, J. Wen, Opt. Express 25 (2017) 9019–9027.
[24] W.M. Robertson, M. May, Appl. Phys. Lett. 74 (1999) 1800–1802.
[25] S. Li, J. Liu, Z. Zheng, Y. Wan, W. Kong, Y. Sun, IEEE Sens. J. 16 (2015) 1200–1204.
[26] Y. Wan, M. Cheng, Z. Zheng, K. Liu, Sensors 19 (2019) 2088.
[27] S. Li, Y. Wan, J. Liu, W. Kong, Z. Zheng, Appl. Sci. 9 (2019) 40.
[28] A. Myc, C. Divin, F.L. Terry, J.R. Baker, J.Y. Ye, T.B. Norris, Y.Y. Jing, Opt. Express 16 (2008) 11741–11749.
[29] Y. Sun, Z. Zheng, J.T. Cheng, J.W. Liu, Opt. Commun. 328 (2014) 124–128.
[30] M. Zhang, J.S. Liu, W.F. Cheng, J.T. Cheng, Z. Zheng, Sensors 19 (2019) 3324.
[31] P. Yeh, A. Yariv, C.-S. Hong, J. Opt. Soc. Amer. B 67 (1977) 423–438.
[32] M.H.P. Pfeiffer, J. Liu, M. Geiselmann, T.J. Kippenberg, Phys. Rev. Appl. 7 (2016) 1–8.
[33] M.L. Gorodetsky, A.A. Savchenkov, V.S. Ilchenko, Proc. SPIE 3267 (1998) 251–262.
[34] Y.Y. Zhou, F. Luan, B. Gu, X. Yu, Opt. Express 23 (2015) 4991–4996.